Journal Pre-proofs

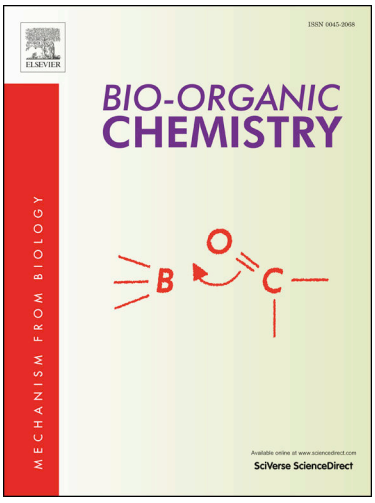

Optimization of activity localization of quinoline derivatives: Design, synthesis, and dual evaluation of biological activity for potential antitumor and antibacterial agents

Guofan Jin, Zhenwang Li, Fuyan Xiao, Xueyong Qi, Xianyu Sun

PII: S0045-2068(19)31551-2
DOI: https://doi.org/10.1016/j.bioorg.2020.103837
Reference: YBIOO 103837

To appear in: *Bioorganic Chemistry*

Received Date: 18 September 2019
Revised Date: 25 December 2019
Accepted Date: 6 April 2020

Please cite this article as: G. Jin, Z. Li, F. Xiao, X. Qi, X. Sun, Optimization of activity localization of quinoline derivatives: Design, synthesis, and dual evaluation of biological activity for potential antitumor and antibacterial agents, *Bioorganic Chemistry* (2020), doi: https://doi.org/10.1016/j.bioorg.2020.103837

This is a PDF file of an article that has undergone enhancements after acceptance, such as the addition of a cover page and metadata, and formatting for readability, but it is not yet the definitive version of record. This version will undergo additional copyediting, typesetting and review before it is published in its final form, but we are providing this version to give early visibility of the article. Please note that, during the production process, errors may be discovered which could affect the content, and all legal disclaimers that apply to the journal pertain.

© 2020 Elsevier Inc. All rights reserved.

Journal Pre-proofs

Optimization of activity localization of quinoline derivatives: Design, synthesis, and dual evaluation of biological activity for potential antitumor and antibacterial agents

Guofan Jin[a,]*, Zhenwang Li[b], Fuyan Xiao[a], Xueyong Qi[b] and Xianyu Sun[a]*

[a]School of Pharmacy, Jiangsu University, Zhenjiang 212013, China

[b]College of Animal Science and Technique, Bayi Agriculture University, Daqing 163319, Heilongjiang, China

*Correspondence:

organicboron@ujs.edu.cn. Tel.: +86-511-8503-8201.

sxianyu@163.com Tel.: +86-459-6819198.

Journal Pre-proofs

Journal Pre-proofs

Abstract

A novel of quarternary amine around a quinolinium iodide combined with even number alkyl chain were prepared in a several step in moderate yield starting from malonic ester and benzo[d][1,3]dioxol-5-amine. All of the active structure compounds were identified by nuclear magnetic resonance (NMR), such as ^{1}H-NMR, ^{13}C-NMR, infrared radiation (IR), high resolution mass spectrometry (HR-MS) and Carlo Erba Instruments CHNS-O EA1108 spectra analysis. With regard to the anticancer properties, the in vitro cytotoxicity against three human cancer cell lines (A-549, Hela and SGC-7901) were evaluated. The antibacterial properties against two human bacterial strains, *Escherichia coli* (ATCC 29213) and *Staphylococcus aureus* (ATCC 8739), along with minimum inhibitory concentration (MIC) values were evaluated. The target compounds, 5–12, exhibited significant antitumor and antibacterial activity, of which compound 12 was found to be the most potent derivative with IC_{50} values of 5.18±0.64, 7.62±1.05, 17.59±0.41, and 54.45±4.88 against A-549, Hela, SGC-7901, and L-02 cells, respectively, stronger than the positive control 5-FU and MTX. Furthermore, compound 12 had the most potent inhibitory activity. The MIC of this compound against *Escherichia coli* (ATCC 29213) and *Staphylococcus aureus* (ATCC 8739) was 3.125 nmol·mL^{-1}, which was smaller than that of the reference agents, amoxicillin and ciprofloxacin.

Keywords: quinolinium iodide; anticancer; antibacterial; human cancer; human bacterial strains

Journal Pre-proofs

1. Introduction

With the continuous development of pharmaceutical, it is becoming increasingly difficult to find new structures to make anti-cancer antibacterial drugs from natural sources [1-3]. Moreover, because these drugs play important roles in clinics, their widespread use and even abuse have led to the evolution of drug-resistant bacteria that pose a threat to human health and survival [4]. This has prompted the development of chemical synthetic drugs. Synthetic chemical drugs still occupy a large proportion compared to biopharmaceuticals and traditional Chinese medicines, and chemical synthetic drugs play a major role in bacterial infections, tuberculosis [5, 6], senile diseases [7, 8], and cancer [10, 11].

Quinolones are chemosynthetic antibacterial drugs discovered by Lesher in 1962, which have been used up to now. Thus far, quinolones have been updated four times [12, 13], and they have been active in people's field of vision owing to their good anticancer, antibacterial activity, broad antibacterial spectrum, and excellent pharmacokinetics [14-18].

Quinolones can induce cell apoptosis by interfering with bacterial DNA replication. Diseases that are made therapeutic with quinolones by this mechanism include urinary infections caused by Escherichia coli, Aerobacter aerogenes, and Pseudomonas aeruginosa, along with Mycoplasma, Chlamydia, and Legionella-induced respiratory infections, such as pneumonia [19, 20]. In addition, they also have good therapeutic effects on the diseases caused by bacterial infections of cocci and Haemophilus, such as chronic bronchitis [21, 22]. On the other hand, with the expansion of the antibacterial spectrum, antibiotics, such as quinolones, have also provided convenience to people and enhanced the bacterial resistance. Therefore, the development of new antibacterial drugs is essential to inhibit the activity of drug-resistant bacteria.

In recent years, there have been many studies on structural modification based on improved antibacterial activity, which has also made great progress in the development of quinolone drugs [23, 24]. On the other hand, to make it have the property of inhibiting DNA TOPO II, quinolones were modified structurally to induce tumor cell apoptosis. There were some studies on the modification with the purpose of implement this mechanism, and new anti-tumor drugs were prepared. For instance, SNS-595 (Voreloxin) is a novel typical compound that was engineered structurally based on the quinolone parent ring and has been patented and entered Phase II clinical research [25-28]. Therefore, quinolones are dual-effect, anti-cancer, and anti-tumor chemical synthetic drugs with great development potential.

Journal Pre-proofs

A literature review showed that the later generations of classical quinolones did not change too much in the 1- and 4- positions. Until now, it still stays on a simple improvement, so its antibacterial and antitumor activity should be enhanced through structural modification to fill the gap in the direction of drug availability. In this paper, further than the existing previous relevant research on general modification of quinolones [29, 30], we introduced secondary amine into quinolone core at 4-position to attach a hydrophobic arylamino group. At the same time, we were interested in the preparation of quarternary amine compounds with alkyliodine substitute on the nitrogen atom at 1-position. The purpose of this study is to synthesize a series of 1- and 4-position modified compounds with ideal antibacterial and anticancer dual activities.

2. Design

Focusing on the quinoline nucleus, modification of the 1- and 4- positions has been considered [31-33]. A strategy for retention was chosen for the small platinum base and ethyl lipid groups of the quinoline nucleus. First, the carbonyl group at the 4-position is often an important part of the hydrogen bond energy level with DNA. The oxygen atom is converted to a secondary amine to increase the binding energy to DNA. In addition, the introduction of an arylamine can increase the lipophilic amine and external binding of the protein increases hydrogen bonding of the quinoline ring π-H ability. Second, the Schiff base tertiary amine of the 1-position is a dynamic self-assembly area of the drug. What's more, according to the structure-activity relationship studies of quinolone drugs in related literatures, the introduction of substituents at position 6 and 7 can significantly enhance the activity, especially the heteroatom ring. Therefore, 1,3-dioxole heterocyclic substitute was retained at 6 and 7-position. To optimize its characteristics, the introduction of iodoethane and iodoisopropane was modified simply to increase the length and specific surface of the branch, and convert it to the quaternary ammonium salt form. Finally, different designs of quinoline and quinolinium iodide salts were proposed to examine their effects on both the anticancer and antibacterial dual activities.The target compound was synthesized according to the outlined synthetic scheme, and the anticancer and antibacterial activities of the derivative were evaluated. The primary design was as follows: 1) a series of novel quinoline derivatives can be developed for the easy synthesis of chemical structures; 2) the hydrogen bonding energy of each active target was analyzed from the docking results (Fig-2), and the different catalytic residues were identified; and 3) the structure was induced by an alkyl iodide salt to increase the anticancer and antibacterial activity (Fig-1).

Fig-1. Schematic diagram of overall design simulation of quinolone derivatives

Journal Pre-proofs

3. Results and Discussion

3.1. Chemistry

The novel 7-(ethoxycarbonyl)-8-(arylamino)-[1,3]dioxolo[4,5 -g]quinolin-5-ium iodide derivatives were synthesized according to Scheme-1. Ethyl-8-chloro-[1,3]dioxolo[4,5-g]quinoline-7-carboxylate [34] intermediate was prepared by the condensation of malonic acid with the corresponding reagent in the presence of the condition through a four step process. The reaction of the intermediate with benzylamine in anhydrous acetonitrile under reflux overnight resulted in the ethyl 8-(aryl)-[1,3]dioxolo[4,5-g]quinolone -7-carboxylate derivatives 1~4. The iodination of 1, 2, 3, and 4 with an excess of iodomethane or iodopropane under reflux provided the target compounds, 5-12, in moderate yield. The chemical structures of all the synthesized new compounds were characterized by ^{1}H NMR, ^{13}C NMR, IR, HRMS, and CHNS-O EA1108.

Scheme-1. General synthetic route of quinolone derivatives

The IR spectrum showed a strong band at 1482-1476 cm^{-1} due to quaternary amine groups in addition to a band at 1400-1500 cm^{-1} assigned to the amine of iodine salt. The ^{1}H NMR spectrum revealed the presence of blunt singlet signals assigned to the -NH- proton at 8.84-10.36 ppm, -N-CH- at 8.95-9.10 ppm, and O-CH_2-O at 6.08-6.10 ppm for two protons. In contrast, iodoalkane substituted derivatives -NH- proton at 10.27-11.59 ppm, the -N^{+}-CH- at 9.07-9.38 ppm, and O-CH_2-O at 6.18-6.29 ppm, respectively. The ^{13}C NMR spectra indicated the ketone functional groups: the presence of singlet signals at 165.9-168.2 ppm corresponding to C=O carbons.

3.2. Biology

3.2.1. Evaluation of cytotoxicity activity in vitro

Compounds 1-12 were assessed for their anti-proliferative activity in four cell lines, namely the human lung cancer cell line (A549), human hela cell line (HeLa), human gastric carcinoma cell line (SGC-7901), normal liver L-02 cell line (L02) by the MTT (3-(4,5-dimethylthiazol-2-yl) -2,5-diphenyltetrazolium bromide) assay [35-41]. The anticancer drug 5-FU (5-fluoro-2,4(1H, 3H)-pyrimidinedione) and MTX (methotrexate) were co-assayed as the positive control. All compounds tested were dissolved in DMSO and then diluted by the culture medium before the treatment of cultured cells.

Journal Pre-proofs

Table-1. In vitro growth inhibitory activity (IC_{50}μM) of compounds 1-12 against human lung cancer cell line (A549), human hela cell line (HeLa), human gastric carcinoma cell line (SGC-7901), normal liver L-02 cell line (L02), and by a MTT assay.

All synthesized 1- and 4-substituted ethyl-8-arylamino-[1,3]dioxolo[4,5-g]quinoline-7-carboxylate and ethyl-8-arylamino-[1,3]dioxolo[4,5-g]quinoliniumiodoalkyl-7-carboxylate derivatives were tested on the human cancer cell line; the data is listed in Table-1. Compared with the non-substituted iodoalkane compounds, all acquired compounds with iodoalkane substitution at the 1-position (8 and 12) showed significantly improved potencies. As for the 4-position substitutions on ethyl-8-arylamino-[1,3]dioxolo[4,5-g]quinoline-7-carboxylate, the effect on the aromatic ring appeared to follow the same rule, it is low activity. This is because the substitution of the 4-position into the bulky-aromatic ring leads to the docking site of NH and DNA to be blocked, which greatly affects the activity of the compound (1~4). Therefore, introduction of branched chains in the aromatic ring site in order to alleviate the steric hindrance, but the effect was still not solved, and obtained very unsatisfactory results. In addition, on the normal hepatocyte cell line (L02) an IC_{50} values of >200 μM, which clearly indicates that the compounds same as the reference drug 5-FU.

As for the various R2, the pyridine ring with an alkyl-iodine substituted at the para-position (5~12) exhibited better potency than non-substituted position (1~4). The para-substituted pyridine ring with an ethyl (8) or isopropy group (12) appeared to contribute concurrently to the potency. In contrast to the other analogs, 12 with aromatic ether substitution at R1 also demonstrated good enzymatic potency. To explore the binding modes of the ethyl-8-arylamino-[1,3]dioxolo[4,5-g]quinoliniumiodoalkyl- 7-carboxylate, one of the most active inhibitors 12 was selected as a representative and docked to the crystal structure of human topoisomerase I (PDB: 1TL8). The docking of 12 in Fig. 3a displayed a free energy of the binding affinity of -8.7 kcal/mol. The binding mode displayed one hydrogen bond acceptor interaction between N at 4-position and base DT10, hydrogen bong donor interaction between carbonyl oxygen and base DG112 in addition to π-π interaction between arylamine-substituted phenyl ring and base DT10. It also exhibited CH-π interaction of quinoline pyridine ring and base DG112 and cation-π interaction of arylamine-substituted phenyl ring and amino acid residue Arg364.

This was also docked to the S. aureus DNA gyrase (Topo II, PDB: 2XCT). The docking of 12 in Fig. 3b displayed a free energy of the binding affinity of -9.2 kcal/mol. 3D binding model showed mainly π-π

interaction between quinolone phenyl ring and base DT8, between quinoline pyridine ring and base DT8 or DG9. Although no hydrogen bond interactions in this model, it is worth mention that cation-π interactions and CH-π interactions played another vital role in binding.

According to the above analysis, compound 12 exhibited significant growth inhibition with an IC_{50} of 5.18±0.64, 7.62±1.05, and 17.59±0.41 against A-549, Hela, and SGC-7901, respectively.

3.2.2. Evaluation of antibacterial activity in vitro

The newly synthesized MIC values of final compounds 1-12 were evaluated for their antibacterial activity against *Escherichia coli* (ATCC 29213) and *Staphylococcus aureus* (ATCC 8739) [42-45]. The test compounds dissolved in DMSO were added to the culture medium (brain heart infusion for *S. mutans* and Müller-Hinton agar for other bacteria) to obtain final concentrations of 1-50 nmol mL^{-1}. A standardized suspension of the test bacterium was inoculated and incubated for 24-48 h at 37 °C, and the lowest concentration of the compounds that prevented the development of visible growth was then analyzed by calculating the minimal inhibitory concentrations (MIC values). Ciprofloxacin and amoxicillin were used as controls and assayed under identical conditions. All experiments were performed in triplicate.

In general, all compounds exhibited promising antibacterial activity against the bacterial strains tested in comparison with the reference drugs. Compounds 8 and 12 showed eight~four times higher antibacterial activity against *E. coli* than ampicillin and ciprofloxacin with MIC values 6.25~3.125 nmol/mL. In addition, these compounds showed eight~four times higher antibacterial activity against *S. aureus* than ampicillin and ciprofloxacin with MIC values of 6.25~3.125 μg/mL. In contrast, compounds 8 and 12 showed higher antibacterial activity against *E. coli* and *S. aureus* to that of ampicillin and ciprofloxacin. In particular, compound 12 showed excellent antibacterial activity. Nevertheless, compounds (1~4) did not show obvious activity compared to the reference drug (Table-2).

Table-2. Antibacterial screening in terms of the MIC (μg/mL**)** for the tested compounds in reference to Ampicillin and Ciprofloxacin, respectively.

3.3. Structure-activity relationship (SAR)

Based on the SAR studies [46] and from the obtained biological results, the un-substituted 1~4 did not exhibit potential anticancer and antibacterial activities. In contrast, alkyliodine substituted at the 1-position showed that pyridine 5~12 with the 4-position *N*-phenyl substituent on quinoline possessed the highest dual activity against all cancer cell and strains tested. The hydrogen at the 1-position was replaced

Journal Pre-proofs

with an alkyliodine group, such as iodoethyl group in 8 and iodoisopropane group in 12, respectively, containing an iodine quaternary ammonium salt group, and the anticancer activity against some cancer cells was more significant than 5-FU and MTX. Moreover, the antibacterial activity against certain strains showed high activity compared to amoxicillin and ciprofloxacin. The conversion of a 4-position carbonyl group to a hydrophobic aromatic amine group to obtain 1-4 compounds, and most of these structures contained a hydrophobic group, and had little effect on the activity of the cancer cells and strains. Accordingly, iodoalkyl was introduced further to obtain 5-12 compounds, exhibiting extremely high activity in terms of double inhibition. In considering of higher activity, compounds 5-12 examined possess a quaternary amino group in the 1-position, leading to a permanent positive charge. In fact, the delocalization of a net positive charge can enhance the membrane permeability. It was therefore significant that we discovered that tertiary amino compounds retained substantial activity, as this broadens development options.

On the other hand, other lipophilic iodo quaternary ammonium salt derivatives are not as strong as expected, and were generally only inhibitory to cancer cells and strains, such as compounds 5, 6, and 7 with 9, 10, and 11, respectively. Although iodomethane and iodopropane were introduced at the same 1-position, and aromatic groups were introduced at the 4-position, the difference in activity exhibited by them was large, and the results were uneven. This type of decrease in activity may be due to the large space conformation, hindered space combined with enzyme-binding pocket conflict, or that the 4-position aromatic amine group hinders the ability to combine with the DNA. Among all the derivatives containing an iodo quaternary ammonium salt group, the compounds substituted at the 1- and 4-positions all exhibited extremely high dual activity. Preliminary synthetic SAR studies [29] have shown that to obtain better dual activity, the 1-position on the mother structure should contain an uneven number of chain hydrophobic groups and the 4-position should contain an uneven number of chain groups to have a positive impact on the structure of dual activity.

3.4. Molecular docking study

AutoDock Vina 1.1.2. software was used to perform docking simulations. In the present study, the derivatives were designed based on the quinoline core, depending on the former studies on the mechanism of anticancer and antibacterial activity [47]. The 3D crystal structure of human topoisomerase I and S. aureus DNA gyrase (Topo II) reported in Protein Data Bank (PDB) were used as the receptor for docking studies (PDB ID: 1TL8, 2XCT) [48-52]. The co-crystallized structure of the target proteins

were downloaded from the PDB and prepared for docking using the docking program AutoDockVina 1.1.2. and MGLTools. The docking result was analyzed and optimized by Pymol 1.5.6. (Fig-2).

Fig 2. 3D binding mode of derivative 12 in the binding site of (a) Human topoisomerase I (PDB ID: 1TL8); (b) *S. aureus* DNA gyrase (Topo II, PDB ID: 2XCT).

The docking of 12 in Fig. 2a displayed a free energy of the binding affinity of -8.7 kcal/mol. The binding mode displayed one hydrogen bond acceptor interaction between N at the 4 position and base DT10, a hydrogen bong donor interaction between the carbonyl oxygen and base DG112, and a π-π interaction between the arylamine-substituted phenyl ring and base DT10. It also exhibited CH-π interaction of the quinoline pyridine ring and base DG112 and the cation-π interaction of arylamine-substituted phenyl ring and amino acid residue Arg364.

Docking of 12 in Fig. 2b showed a free energy of binding affinity of -9.2 kcal/mol. The 3D binding model showed mainly the π-π interaction between the quinolone phenyl ring and base DT8 between quinoline pyridine ring and base DT8 or DG9. Although there were no hydrogen bond interactions in this model, the cation-π interactions and CH-π interactions showed another vital role in binding.

4. Experimental

4.1. Materials and Methods

All solvents and reagents were commercially purchased and used as received and employed further purification. Moisture-sensitive reactions were performed under nitrogen atmosphere. acetonitrile was distilled over calcium hydride. All glassware including needles and syringes were torch flame or oven-dried and kept in a desiccator before use. The reaction products were isolated and purified by column chromatography (silica gel 200~230 mesh). Thin-layer chromatography (TLC) was used to monitor the progress of the reaction. Analysis of TLC results at 254 nm and 360 nm wavelengths under UV lamps. Characterization of the products at each stage by NMR spectroscopy, ^{1}H, and ^{13}C NMR spectra were recorded on Bruker Avance II spectrometer in $CDCl_3$ (400 MHz for ^{1}H and100 MHz for ^{13}C); chemical shifts are expressed in ppm, versus internal tetramethylsilane (TMS) = 0 for ^{1}H and ^{13}C. Coupling constants (*J*) are given in Hz. Elemental analyses were performed using a Carlo Erba Instruments CHNS-O EA1108 analyser. IR spectra of samples were recorded on a Nicolet avato-370 FT-IR analyzer using KBr disks. Carlo Erba Instruments CHNS-O EA1108 analyser and HR-MS (FAB) (Jeol LTD JMS-HX 110/110A) were performed by the Chosun University of the Republic of Korea.

4.2. General Procedure for the Synthesis of 1-4

Ethyl 8-chloro-[1,3]dioxolo[4,5-g]quinoline-7- carboxylate (1.0 eq.) was added to a solution of the arylamine compound (2.5 eq.) in dry acetonitrile (10 mL) and stirred at 80°C for 8-10 h. Thin layer chromatography was used to monitor the progress of the reaction. The solvent was added to 10 mL water with 5 mL dichloromethane and extracted 3 times. The organic layer was dried anhydrous magnesium sulfate and filtered. The residue was purified by column chromatography (EtOAc:petroleum ether = 1:8) to produce a yellowish solid.

Ethyl 8-(benzylamino)-[1,3]dioxolo[4,5-g]quinoline-7-carboxylate **1**

A yellowish solid (1.0 g, 79.2%): ^{1}H NMR (400MHz, $CDCl_3$, ppm): δ 9.15 (s, 1H), 9.01 (s, 1H), 7.47 (s, 1H), 7.41-7.34 (m, 6H), 6.09 (s, 2H), 4.89 (d, J = 6.4 Hz, 2H), 4.39 (dd, J = 6.8 Hz, 2H), 1.42 (t, J = 6.8 Hz, 3H). ^{13}C NMR (100MHz, $CDCl_3$, ppm): δ 168.6, 156.5, 151.3, 149.9, 149.7, 146.2, 138.6, 129.0, 128.9, 127.8, 127.1, 114.9, 106.7, 104.4, 101.9, 60.7, 52.5, 14.3.

Ethyl 8-(phenethylamino)-[1,3]dioxolo[4,5-g]quinoline-7-carboxylate **2**

A yellow solid (1.1 g, 84.8%): ^{1}H NMR (400MHz, $CDCl_3$, ppm): δ 8.96 (s, 1H), 8.87 (s, 1H,), 7.47 (s, 1H), 7.33–7.25 (m, 6H), 6.10 (s, 2H), 4.40–4.35 (m, 2H), 3.99-3.94 (m, 2H), 3.05 (t, J = 7.2 Hz, 2H), 1.44 (t, J = 7.2 Hz, 3H). ^{13}C NMR (100MHz, $CDCl_3$, ppm): δ 168.6, 156.4, 151.2, 150.0, 149.6, 146.0, 138.1, 128.8, 128.6, 126.8, 115.0, 106.7, 104.0, 102.0, 101.9, 60.6, 50.7, 37.6, 14.4.

Ethyl 8-((3,4-dimethoxyphenethyl)amino)-[1,3]dioxolo[4,5-g]quinoline-7-carboxylate **3**

A yellowish solid (1.3 g, 85.0%): ^{1}H NMR (400MHz, $CDCl_3$, ppm): δ 8.95 (s, 2H), 7.50 (s, 1H), 7.32 (s, 1H), 6.83–6.81 (m, 3H), 6.11 (s, 2H), 4.37 (dd, J = 7.2 Hz, 2H), 3.97 (m, 2H), 3.90 (d, J = 6.8 Hz, 6H), 3.00 (t, J = 7.2 Hz, 2H), 1.43 (t, J = 7.2 Hz, 3H). ^{13}C NMR (100MHz, $CDCl_3$, ppm): δ 166.6, 156.4, 151.3, 149.8, 149.5, 149.0, 147.9, 146.0, 130.7, 120.7, 115.0, 112.3, 111.5, 106.7, 103.8, 102.1, 102.0, 60.6, 55.9, 55.8, 50.9, 37.2, 14.3.

Ethyl 8-((4-(benzyloxy)phenyl)amino)-[1,3]dioxolo[4,5-g]quinoline-7-carboxylate **4**

A yellowish solid (1.2 g, 70.0%): ^{1}H NMR (400MHz, $CDCl_3$, ppm): δ 10.37 (s, 1H), 9.10 (s, 1H)，7.48–7.36 (m, 6H), 7.02–6.90 (m, 5H), 6.05 (s, 2H), 5.08 (s, 2H), 4.44 (d, J = 6.8 Hz, 2H), 1.47 (t, J = 7.2 Hz, 3H). ^{13}C NMR (100MHz, $CDCl_3$, ppm): δ 168.5, 156.1, 152.3, 151.6, 149.4, 149.0, 146.1, 136.8, 135.8, 128.6, 128.0, 127.5, 124.1, 115.7, 115.1, 106.1, 102.7, 101.9, 70.4, 61.1, 50.4, 14.3.

4.3. General Procedure for the Synthesis of 5-12.

Journal Pre-proofs

Excess of iodoalkane (5.0 equiv.) was slowly added to a dry acetonitrile (5 mL) solution of compound 7-(ethoxycarbonyl)-8-(arylamino)-[1,3]dioxolo[4,5-g]quinoline (1.0 equiv.) under nitrogen purged in seal tube, and was stirred for 2–4 h. The precipeted solide was filtered, to produce the correspondence compound 5-12.

8-(benzylamino)-7-(ethoxycarbonyl)-5-methyl-[1,3]dioxolo[4,5-g]quinolin-5-ium iodide **5**

A yellow solid (0.2 g, 48%) yield. IR (KBr pellet, cm^{-1}): *v* (N^+) 1478 (strong br). ^1H NMR (400MHz, $CDCl_3$, ppm): *δ* 10.64 (s, 1H), 9.29 (s, 1H), 7.78 (s, 1H), 7.48-7.39 (m, 6H), 6.30 (s, 2H), 5.14 (d, *J* = 5.6 Hz, 2H), 4.90 (dd, *J* = 7.2 Hz, 2H), 4.46 (dd, *J* = 7.2 Hz, 2H), 1.66 (t, *J* = 7.2 Hz, 3H), 1.48 (t, *J* = 7.2 Hz, 3H). ^{13}C NMR (100MHz, $CDCl_3$) *δ* 165.9, 155.1, 148.1, 146.2, 138.0, 135.5, 133.2, 129.4, 128.8, 127.5, 114.5, 104.7, 104.3, 103.1, 97.6, 62.9, 52.5, 15.3, 14.8, 14.4. HR-MS (FAB) calcd for $C_{21}H_{21}IN_2O_4$ (M^+- I^-) *m/z* 379.1611, observed 379.1605. Calcd for $C_{22}H_{23}IN_2O_4$: C, 52.19; H, 4.58; N, 5.53. Found: C, 52.13; H, 4.55; N, 5.59.

7-(ethoxycarbonyl)-5-methyl-8-(phenethylamino)-[1,3]dioxolo[4,5-g]quinolin-5-ium iodide **6**

A yellow solid (0.38 g, 90%) yield. IR (KBr pellet, cm^{-1}): *v* (N^+) 1478 (strong br). ^1H NMR (400MHz, $CDCl_3$, ppm): *δ* 10.33 (t, *J* = 0.8 Hz, 1H), 9.20-9.13 (m, 1H), 7.74 (s, 1H), 7.33-7.27 (m, 5H), 6.29 (s, 2H), 4.83-4.78 (m, 2H), 4.46-4.40 (m, 2H), 4.19 (d, *J* = 5.2 Hz, 2H), 3.14 (t, *J* = 6.8 Hz, 2H), 1.62-1.55 (m, 3H), 1.50-1.41 (m, 3H). ^{13}C NMR (100 MHZ, $CDCl_3$) *δ* 165.9, 157.3, 155.0, 147.9, 146.2, 137.8, 136.7, 128.9, 128.9, 127.3, 114.7, 104.6, 104.2, 102.9, 97.5, 62.8, 52.3, 50.9, 36.6, 14.8, 14.5. HR-MS (FAB) calcd for $C_{22}H_{23}IN_2O_4$ (M^+-I^-) *m/z* 393.1814, observed 393.1808. Calcd for $C_{23}H_{25}IN_2O_4$: C, 53.09; H, 4.84; N, 5.38. Found: C, 53.11; H, 4.89; N, 5.55.

8-((3,4-dimethoxyphenethyl)amino)-7-(ethoxycarbonyl)-5-methyl-[1,3]dioxolo[4,5-g]quinolin-5-ium iodide **7**

A yellow solid (0.38 g, 94%) yield. IR (KBr pellet, cm^{-1}): *v* (N^+) 1483 (strong br). ^1H NMR (400MHz, $CDCl_3$, ppm): *δ* 10.36 (s, 1H), 9.21 (s, 1H), 7.78 (s, 1H), 7.43 (s, 1H), 6.85 (s, 3H), 6.30 (s, 2H), 4.84 (d, *J* = 6.8 Hz, 2H), 4.46 (d, *J* = 7.2 Hz, 2H), 4.19 (s, 2H), 3.91 (d, *J* = 16.4 Hz, 6H), 3.10 (s, 2H), 1.63 (t, *J* = 7.2 Hz, 3H), 1.51 (t, *J* = 7.2 Hz, 3H). ^{13}C NMR (100MHz, $CDCl_3$) *δ* 165.9, 155.0, 149.1, 148.1, 147.9, 146.1, 137.8, 129.3, 121.0, 114.6, 114.6, 112.5, 111.6, 104.8, 104.2, 102.7, 97.4, 62.7, 56.1, 56.0, 52.3, 51.3, 36.1, 14.8, 14.5. HR-MS (FAB) calcd for $C_{24}H_{27}IN_2O_6$ (M^+- I^-) *m/z* 453.2014, observed 453.2012. Calcd for $C_{25}H_{29}IN_2O_6$: C, 51.73; H, 5.04; N, 4.83. Found: C, 51.81; H, 5.12; N, 4.85.

Journal Pre-proofs

8-((4-(benzyloxy)phenyl)amino)-7-(ethoxycarbonyl)-5-methyl-[1,3]dioxolo[4,5-g]quinolin-5-ium iodide **8**

A yellow solid (0.16 g, 39%) yield. IR (KBr pellet, cm^{-1}): *v* (N^+) 1474 (strong br). ^1H NMR (400MHz, $CDCl_3$, ppm): δ 11.68 (s, 1H), 9.50 (s, 1H), 7.48-7.41 (m, 6H), 7.24 (d, *J* = 8.8 Hz, 2H), 7.07 (d, *J* = 6.8 Hz, 3H), 6.21 (s, 2H), 5.12 (s, 2H), 5.00 (d, *J* = 7.2 Hz, 2H), 4.51 (d, *J* = 7.2 Hz, 2H), 1.71 (t, *J* = 7.2 Hz, 3H), 1.55 (t, *J* = 7.2 Hz, 3H). ^{13}C NMR (100MHz, $CDCl_3$) δ 166.2, 158.3, 155.2, 154.8, 147.6, 146.6, 138.3, 136.2, 131.5, 128.2, 128.2, 127.5, 126.0, 116.5, 114.5, 104.5, 104.2, 104.0, 97.5, 70.4, 63.1, 52.8, 15.1, 14.5. HR-MS (FAB) calcd for $C_{27}H_{25}IN_2O_5$ (M^+- I^-) *m/z* 471.1920, observed 471.1911. Calcd for $C_{28}H_{27}IN_2O_5$: C, 56.20; H, 4.55; N, 4.68. Found: C, 56.25; H, 4.61; N, 4.73.

8-(benzylamino)-7-(ethoxycarbonyl)-5-propyl-[1,3]dioxolo[4,5-g]quinolin-5-ium iodide **9**

A white powder (0.31 g, 70%) yield. IR (KBr pellet, cm^{-1}): *v* (N^+) 1485 (strong br). ^1H NMR (400MHz, $CDCl_3$, ppm): δ 10.50 (s, 1H), 8.80 (s, 1H), 7.80 (s, 1H), 7.41-7.35 (m,6H), 6.27 (s, 2H), 5.29 (s, 2H), 5.14 (d, *J* = 4.8 Hz, 1H), 4.42-4.37 (m, 2H), 1.72 (t, *J* = 6.4 Hz, 6H), 1.40 (t, *J* = 7.2 Hz, 3H). ^{13}C NMR (100 MHZ, $CDCl_3$), δ 165.6, 155.4, 148.8, 148.1, 141.2, 135.6, 129.3, 128.3, 127.6, 115.1, 114.9, 114.8, 104.7, 104.2, 98.0, 62.8, 55.9, 53.5, 22.5, 14.2. HR-MS (FAB) calcd for $C_{23}H_{25}IN_2O_4$ (M^+- I^-) *m/z* 393.1811, observed 393.1807. Calcd for $C_{23}H_{25}IN_2O_4$: C, 53.09; H, 4.84; N, 5.38. Found: C, 53.14; H, 4.89; N, 5.40.

7-(ethoxycarbonyl)-8-(phenethylamino)-5-propyl-[1,3]dioxolo[4,5-g]quinolin-5-ium iodide **10**

A white powder (0.31 g, 71%) yield. IR (KBr pellet, cm^{-1}): *v* (N^+) 1485 (strong br). ^1H NMR (400MHz, $CDCl_3$, ppm): δ 10.17 (d, *J* = 0.4Hz, 1H), 8.71 (s, 1H), 7.79 (s, 2H), 7.27-7.21 (m, 5H), 6.25 (s, 2H), 5.47 (t, *J* = 6.0 Hz, 1H), 4.44-4.39 (m, 2H), 4.18 (s, 2H), 3.14 (t, *J* = 6.8 Hz, 2H), 1.67 (d, *J* = 6.4 Hz, 6H), 1.42 (t, *J* = 7.2 Hz, 3H). ^{13}C NMR (100 MHz, $CDCl_3$), δ 165.5, 157.0, 155.2, 147.9, 141.1, 138.1, 136.8, 128.9, 128.7, 127.1, 114.8, 114.7, 104.5, 104.2, 103.0, 97.8, 62.7, 55.7, 50.9, 36.5, 22.5, 14.3. HR-MS (FAB) calcd for $C_{24}H_{27}IN_2O_4$ (M^+- I^-) *m/z* 407.1968, observed 407.1963. Calcd for $C_{24}H_{27}IN_2O_4$: C, 53.94; H, 5.09; N, 5.24. Found: C, 53.92; H, 5.11; N, 5.26.

8-((3,4-dimethoxyphenethyl)amino)-7-(ethoxycarbonyl)-5-propyl-[1,3]dioxolo[4,5-g]quinolin-5-ium iodide **11**

A white powder (0.27 g, 63%) yield. IR (KBr pellet, cm^{-1}): *v* (N^+) 1488 (strong br). ^1H NMR (400MHz, $CDCl_3$, ppm): δ 10.24 (s, 1H), 8.75 (s, 1H), 7.74 (s, 2H), 6.92-6.85 (m, 3H), 6.29 (s, 2H), 5.31 (s, 1H), 4.50-4.42 (m, 2H), 4.22 (s, 2H), 3.91-3.86 (m, 6H), 3.13-3.10 (m, 2H), 1.72 (d, *J* = 6.4 Hz, 6H), 1.46 (t,

Journal Pre-proofs

J = 7.2 Hz, 3H). ^{13}C NMR (100 MHz, $CDCl_3$), δ 165.7.158.7, 153.2, 149.1, 148.1, 147.8, 141.1, 129.3, 126.7, 120.9, 114.9, 112.5, 111.5, 104.7, 104.1, 102.8, 97.8, 62.6, 56.0, 55.9, 51.4, 36.1, 22.5, 14.2. HR-MS (FAB) calcd for $C_{26}H_{31}IN_2O_6$ (M^+- I^-) *m/z* 467.2176, observed 467.2174. Calcd for $C_{26}H_{31}IN_2O_6$: C, 52.53; H, 5.26; N, 4.71. Found: C, 52.54; H, 5.22; N, 4.73.

8-((4-(benzyloxy)phenyl)amino)-7-(ethoxycarbonyl)-5-propyl-[1,3]dioxolo[4,5-g]quinolin-5-ium iodide **12**

A white powder (0.32 g, 77%) yield. IR (KBr pellet, cm^{-1}): *v* (N^+) 1479 (strong br). ^{1}H NMR (400MHz, $CDCl_3$, ppm): δ 11.57 (s, 1H), 8.95 (s, 1H), 7.79 (s, 1H), 7.44-7.33 (m, 5H), 7.25-7.22 (m, 2H), 7.10-7.02 (m, 3H), 6.19 (s, 2H,), 5.59 (t, *J* = 6.4 Hz, 1H), 5.09 (s, 2H), 4.48 (dd, *J* = 7.2 Hz, 2H), 1.79 (d, *J* = 6.4 Hz, 6H), 1.47 (t, *J* = 7.2 Hz, 3H). ^{13}C NMR (100 MHz, $CDCl_3$), δ 165.9, 158.2, 155.4, 154.5, 147.6, 141.6, 138.8, 136.2, 131.6, 128.6, 128.1, 127.5, 125.8, 116.4, 114.8, 104.5, 104.1, 104.0, 98.0, 70.4, 63.0, 56.4, 22.7, 14.2. HR-MS (FAB) calcd for $C_{29}H_{29}IN_2O_5$ (M^+- I^-) *m/z* 485.2068, observed 485.2064. Calcd for $C_{29}H_{29}IN_2O_5$: C, 56.87; H, 4.77; N, 4.57. Found: C, 56.90; H, 4.78; N, 4.59.

4.4. In vitro cytotoxicity

The three cancer cell lines, A549, SGC-7901, and Hela, and normal cell lines, normal liver L-02 cells, were acquired from the American Type Culture Collection (Manassas, VA, USA). A549 and SGC-7901 cells were cultured routinely in RPMI-1640, and Hela and L-02 cells were cultured routinely in DMEM [53]. The medium was supplemented with 10% fetal bovine serum (FBS). The cells were maintained at sub-confluence at 37^{o}C in humidified air containing 5% CO_2. The cells were monitored daily and maintained at an 80% cell density.

The cytotoxicity of the tested samples was measured against each cell line using the MTT Cell Viability Cancer cells (A549, SGC-7901 and Hela) and normal human lung L-02 were harvested during the logarithmic phase of growth. All the cells were seeded in 96-well plates at 10^4 cells/well and then treated with various concentrations (1, 3, 10, 30, or 100 μmol/mL) of 5-FU, methotrexate and the tested samples for 24 h. The MTT solution (20 μL; 5 mg/mL) was added to each well, and the cells were cultured for 4 h at 37^{o}C. The supernatants were removed, and resolved with 100 μL of DMSO, and the cells were shocked for 10 min. The optical density of the samples was measured at 490 nm on a microplate luminometer. The cell viability is expressed as the percentage change in absorbance compared to the control values.

4.5. In vitro antimicrobial evaluation

Journal Pre-proofs

The synthetic compounds **1-12** against two bacterial strains were measured using the broth microdilution method in 96-well plates, and the MIC values were determined. The MIC is defined as the lowest concentration of test sequences that completely inhibit growth. The microorganisms used in the present study were *S. aureus* (ATCC 29213) and *E. coli* (ATCC 8739). This was placed on the inoculated muller-Hinton agar plates, and the test compounds were dissolved in DMSO to obtain final concentrations of 1-50 nmol.mL^{-1}. The final bacterial concentration was approximately 10^6 CFU mL^{-1}. The MIC values were measured after incubation for 24 h at 37 °C. Ciprofloxacin and amoxicillin were used as controls and assayed under identical conditions. All experiments were performed in triplicate.

4.6. Molecular docking

AutoDock Vina software package version 1.1.2 was used to perform docking simulations.

Conclusions

In this paper, a series of quinoline derivatives have been synthesized, and their activity patterns were compared between the free form and quaternary ammonium salt forms. In the 4-position selection, arylamine or other aromatic amines were selected as candidates, and in the case of the 1-position, a relatively simple iodoalkyl group was selected as a candidate for modification. The two players have a greater difference in the activity of the parent structure. The novel quinolone structural modification at the 4-position replaced the chlorine atom with an arylamino, possessed only poor activity in this assay. Nevertheless, the further modification of the alkyl-iodide at the N-1 position greatly increased the antibacterial activity as a whole. Therefore, the tertiary amino compounds we synthesized retained substantial activity, which provided broader development options. What's more, it was significant discovered that the 4-position odd-numbered arylamine groups were more active than the even-numbered arylamine groups, particularly the even-numbered arylamine groups with dioxygen atoms showing the lowest pharmaceutically active activity (6 and 10; IC_{50}>120), whereas compound 12 shows the highest activity. Compound 12 showed high toxicity in the normal cell system, which needs to be solved. In the process of drug synthesis and design, selecting and locating the optimal structure-activity relationship does not depend on the number of oxygen and nitrogen atoms, but rationally match their overall distribution and optimization.

Acknowledgements

This study was supported financially by the scientific research foundation of Jiangsu University (Grant No. 5501290005).

Journal Pre-proofs

Conflict of interest

The authors declare that there are no conflicts of interest.

References

1. Q. Guo, H. Cao, X. Qi, Research Progress in Reversal of Tumor Multi-drug Resistance via Natural Products. Anti-Cancer Agents in Medicinal Chemistry. 17 (2017) 1466-1476. doi:10.2174/1871520617666171016105704.
2. A. Dasgupta, D. Dey, D. Ghosh, Astrakurkurone, a Sesquiterpenoid from Wild Edible Mushroom, Targets Liver Cancer Cells by Modulating Bcl-2 Family Proteins. IUBMB Life. 71 (2019) 992-1002. doi:10.1002/iub.2047.
3. R.H. Baltz, Natural product drug discovery in the genomic era: realities, conjectures, misconceptions, and opportunities. J Ind Microbiol Biotechnol. 46 (2019) 281-299. doi:10.1007/s10295-018-2115-4.
4. A. Deb, R. Vimala, Natural and synthetic polymer for graphene oxide mediated anticancer drug delivery-A comparative study. International Journal of Biological Macromolecules. 107 (2018) 2320-2333. doi:10.1016/j.ijbiomac.2017.10.119.
5. M.S. Ahmed, T. Annamalai, X. Li, Synthesis of antimicrobial Poly(guanylurea)s. Bioconjugate Chem. 29 (2018) 1006-1009. doi:10.1021/acs.bioconjchem.8b00057.
6. R. Namivandi-Zangeneh, Z. Sadrearhami, D. Dutta, M. Willcox, E.H.H. Wong, C. Boyer, Synergy between Synthetic Antimicrobial Polymer and Antibiotics: A Promising Platform To Combat Multidrug-Resistant Bacteria. Acs Infectious Diseases. 5 (2019) 1357-1365. doi:10.1021/acsinfecdis.9b00049.
7. S.B. Menon, A. Rahimmemon, A.A. Arain, S.A. Pandhiani, S. Kazi, Co-enzyme Q-10: preventive effects in inh induced hepatotoxicity in albino wistar rats. Indo Am J Pharm Sci. 5 (2018) 15887-15890. doi:10.5281/zenodo.2166702.
8. I. Muramatsu, J. Uwada, H. Yoshiki, Novel regulatory systems for acetylcholine release in rat striatum and anti-Alzheimer's disease drugs. J Neurochem. 149 (2019) 605-623. doi:10.1111/jnc.14701.
9. P. Paudel, S.H. Seong, Y. Zhou, H.J. Park, H.A. Jung, J.S. Choi, Anti-Alzheimer's Disease Activity of Bromophenols from a Red Alga, Symphyocladia latiuscula (Harvey) Yamada. ACS Omega. 4 (2019) 12259-12270. doi:10.1021/acsomega.9b01557.
10. M. Huo, Y. Zhao, A.B. Satterlee, Y. Wang, Y. Xu, L. Huang, Tumor-targeted delivery of sunitinib base enhances vaccine therapy for advanced melanoma by remodeling the tumor microenvironment. Journal of Controlled Release. 245 (2017) 81-94. doi:10.1016/j.jconrel.2016.11.013.
11. W. Zhu, D. Li, X. Li, Association between adjuvant docetaxel-based chemotherapy and breast cancer-related lymphedema. Anti-Cancer Drugs. 28 (2017) 350-355. doi:10.1097/cad.0000000000000468.
12. X. Guo, C. Kang, H. Huang, Y. Chang, C. Zhong, Exploration of functional MOFs for efficient removal of fluoroquinolone antibiotics from water. Microporous and Mesoporous Materials. 286 (2019) 84-91. doi:10.1016/j.micromeso.2019.05.025.
13. D.R. Morales, R. Flynn, X. Kurz, Addendum to: Relative and Absolute Risk of Tendon Rupture with Fluoroquinolone and Concomitant Fluoroquinolone/Corticosteroid Therapy: Population-Based Nested Case-Control Study. Clinical Drug Investigation. 39 (2019) 591-594. doi:10.1007/s40261-019-00792-7.
14. L.-H. Hang, Z.-K. Xu, S.-Y. Wei, W.-W. Shu, H. Luo, J. Chen, Spinal SET7/9 may contribute to the maintenance of cancer-induced bone pain in mice. Clinical and Experimental Pharmacology and Physiology. 44 (2017) 1001-1007. doi:10.1111/1440-1681.12789.

Journal Pre-proofs

15. Y.-L. Fan, X.-W. Cheng, J.-B. Wu, Antiplasmodial and antimalarial activities of quinolone derivatives: An overview. Eur J Med Chem. 146 (2018) 1-14. doi:10.1016/j.ejmech.2018.01.039.
16. I. Ali, M. Suhail, L. Asnin, Chiral separation of quinolones by liquid chromatography and capillary electrophoresis. J Sep Sci. 40 (2017) 2863-2882. doi:10.1002/jssc.201700200.
17. C. Gao, Y.-L. Fan, F. Zhao, Quinolone derivatives and their activities against methicillin-resistant Staphylococcus aureus (MRSA). Eur J Med Chem. 157 (2018) 1081-1095. doi:10.1016/j.ejmech.2018.08.061.
18. S. Xu, F. Ye, L. Li, Ghrelin attenuates vascular calcification in diabetic patients with amputation. Biomedicine & Pharmacotherapy. 91 (2017) 1053-1064. doi:10.1016/j.biopha.2017.05.031.
19. M. Tellis, J. Joseph, H. Khande, S. Bhagwat, M. Patel, In vitro bactericidal activity of levonadifloxacin (WCK 771) against methicillin- and quinolone-resistant Staphylococcus aureus biofilms. Journal of Medical Microbiology. 68 (2019) 1129-1136. doi:10.1099/jmm.0.000999.
20. B.-B. Miao, X.-H. Yang, B.-B. Liang, J.-S. Jia, J. Wang, R. Wang, Antibacterial Activity of Three Quinolones Against Staphylococcus aureus in Vitro. Zhongguo Yaoxue Zazhi (Beijing, China). 52 (2017) 1241-1245. doi:10.11669/cpj.2017.14.009
21. L. Dellgren, C. Claesson, M. Hogdahl, Phenotypic screening for quinolone resistance in Escherichia coli. European Journal of Clinical Microbiology & Infectious Diseases. 38 (2019) 1765-1771. doi:10.1007/s10096-019-03608-w.
22. X. Yu, J. Zhang, J. Zhang, Photocatalytic degradation of ciprofloxacin using Zn-doped Cu2O particles: Analysis of degradation pathways and intermediates. Chemical Engineering Journal. 374 (2019) 316-327. doi:10.1016/j.cej.2019.05.177.
23. S.A. Khan, A.M. Asiri, M.Y. Wani, K.S. Sharma, M. Asad, Synthesis and evaluation of Quinoline-3-carbonitrile derivatives as potential antibacterial agents. Bioorganic Chemistry. 88 (2019) 102968. doi:10.1016/j.bioorg.2019.102968.
24. S. A. Khan, Green Synthesis, Spectrofluorometric Characterization and Antibacterial Activity of Heterocyclic Compound from Chalcone on the Basis of in vitro and Quantum Chemistry Calculation. Journal of Fluorescence. 27 (2017) 929-937. doi: 10.1007/s10895-017-2028-z.
25. G.L. Gravina, A. Mancini, C. Mattei, Enhancement of radiosensitivity by the novel anticancer quinolone derivative vosaroxin in preclinical glioblastoma models. Oncotarget. 8 (2017) 29865-29886. doi:10.18632/oncotarget.16168.
26. H. Sayar, P. Bashardoust, Therapies for acute myeloid leukemia: vosaroxin. Oncotargets and Therapy. 10 (2017) 3957-3963. doi:10.2147/ott.s121477.
27. A.-U. Zaman, I. Ahmad, M. Pervaiz, A novel synthetic approach for the synthesis of pyrano 3,2-c quinolone-3carbaldehydes by using modified Vilsmeier Haack reaction, as potent antimicrobial agents. Journal of Molecular Structure. 1180 (2019) 227-236. doi:10.1016/j.molstruc.2018.11.030.
28. R.M. Lima, K.C. Souza, J.D.A. Lazzarini, I.O. Souza, A.D. Silva, N.R. Barbosa Raposo, Quinoline Derivatives as Novel Depigmenting and Antioxidant Agents. Letters in Drug Design & Discovery. 14 (2017) 374-379. doi:10.2174/1570180813666160930164926.
29. R. Wang, K. Xu,W.X. Shi, Quinolone derivatives: Potential anti-HIV agent-development and application. Archiv Der Pharmazie. 352 (2019) 1900045. doi: 10.1002/ardp.201900045.
30. S.C. Teguh, N. Klonis, S. Duffy, L. Lucantoni, V.M. Avery, C.A. Hutton, J.B. Baell, L. Tilley, Novel Conjugated Quinoline-Indoles Compromise Plasmodium falciparum Mitochondrial Function and Show Promising Antimalarial Activity. Journal of Medicinal Chemistry. 56 (2013) 6200-6215. doi: 10.1021/jm400656s.

Journal Pre-proofs

31. S.-H. Kwak, S. Shin, J.-H. Lee, Synthesis and structure-activity relationships of quinolinone and quinoline-based P2X7 receptor antagonists and their anti-sphere formation activities in glioblastoma cells. European Journal of Medicinal Chemistry. 151 (2018) 462-481. doi:10.1016/j.ejmech.2018.03.023.
32. R.M. Abdelhameed, R.A. Ismail, M. El-Naggar, E.S. Zarie, R. Abdelaziz, M.T. Sayed, Post-synthetic modification of MIL-125 with bis-quinoline Mannich bases for removal of heavy metals from wastewater. Microporous and Mesoporous Materials. 279 (2019) 26-36. doi:10.1016/j.micromeso.2018.12.018.
33. H. Xu, P. Wang, Q. Qin, R. Zhao, G. Huang, Effect of surface modification on quinoline adsorption onto coking coal. Desalination and Water Treatment. 159 (2019) 282-289. doi:10.5004/dwt.2019.24138.
34. R.D. Larsen, D. Cai, Product class 3: quinolines. Science of Synthesis. 15 (2005) 389-549.
35. H. Qiu, L. Zhang, M. Zhu, Capture of anti-coagulant active ingredients from Moutan Cortex by platelet immobilized chromatography and evaluation of anticoagulant activity in rats. Biomedicine & Pharmacotherapy. 95 (2017) 235-244. doi:10.1016/j.biopha.2017.08.051.
36. X. Du, P. Zhang, H. Fu, H.M. Ahsan, J. Gao, Q. Chen, Smart mitochondrial-targeted cancer therapy: Subcellular distribution, selective TrxR2 inhibition accompany with declined antioxidant capacity. International Journal of Pharmaceutics. 555 (2019) 346-355. doi:10.1016/j.ijpharm.2018.11.057.
37. H.-Y. Zhang, C.- Y. Sun, M. Adu-Frimpong, J.-N. Yu, X.-M. Xu, Glutathione-sensitive PEGylated curcumin prodrug nanomicelles: Preparation, characterization, cellular uptake and bioavailability evaluation. International Journal of Pharmaceutics. 555 (2019) 270-279. doi:10.1016/j.ijpharm.2018.11.049.
38. D. Shang, Y. Wu, Y. Ding, Identification of a pyridine derivative inducing senescence in ovarian cancer cell lines via P21 activation. Clinical and Experimental Pharmacology and Physiology. 45 (2018) 452-460. doi:10.1111/1440-1681.12891.
39. J. Lu, Z. Zhou, M. Tang, Role of LKB1 in migration and invasion of Cr(VI)-transformed human bronchial epithelial Beas-2B cells. Anti-Cancer Drugs. 29 (2018) 660-673. doi:10.1097/cad.0000000000000638.
40. Y. Shen, Y. Yu, B. Chaurasiya, Stability, safety, and transcorneal mechanistic studies of ophthalmic lyophilized cyclosporine-loaded polymeric micelles. Int J Nanomed. 13 (2018) 8281-8296. doi:10.2147/ijn.s173691.
41. X. Luo, H. Zhang, Y. Duan, G. Chen, Protective effects of radish (Raphanus sativus L.) leaves extract against hydrogen peroxide-induced oxidative damage in human fetal lung fibroblast (MRC-5) cells. Biomedicine & Pharmacotherapy. 103 (2018) 406-414. doi:10.1016/j.biopha.2018.04.049.
42. R. Al-Tohamy, S.S. Ali, K. Saad-Allah, Phytochemical analysis and assessment of antioxidant and antimicrobial activities of some medicinal plant species from Egyptian flora. Journal of Applied Biomedicine. 16 (2018) 289-300. doi:10.1016/j.jab.2018.08.001.
43. U. Olgun, K. Tunc, A. Hos, Preparation and antibacterial properties of nano biocomposite Poly(ε-caprolactone)-SiO2 films with nanosilver. J Polym Res. 26 (2019) 1-8. doi:10.1007/s10965-018-1686-0.
44. T. Kawai, I. Kazuhiko, N. Takaya, Sulfonamide-based non-alkyne LpxC inhibitors as Gram-negative antibacterial agents. Bioorg Med Chem Lett. 27 (2017) 1045-1049. doi:10.1016/j.bmcl.2016.12.059.
45. W. Xia, M. Xie, X. Feng, L. Chen, Y. Zhao, Surface modification of poly(vinylidene fluoride) ultrafiltration membranes with chitosan for anti-fouling and antibacterial performance. Macromol Res. 26 (2018) 1225-1232. doi:10.1007/s13233-019-7019-2.
46. G. Abbas, Z. Hassan, A. Al-Harrasi, A. Khan, A. Al-Adawi, M. Ali, Synthesis, biological evaluation, molecular docking and structure-activity relationship studies of halogenated quinone and naphthoquinone derivatives. Journal of Molecular Structure. 1195 (2019) 462-469. doi:10.1016/j.molstruc.2019.06.002.

Journal Pre-proofs

47. J. Panmanee, J. Bradley-Clarke, J.M. Mato, P.M. O'Neill, S.V. Antonyuk, S.S. Hasnain, Control and regulation of S-Adenosylmethionine biosynthesis by the regulatory beta subunit and quinolone-based compounds. Febs Journal. 286 (2019) 2135-2154. doi:10.1111/febs.14790.
48. O. Trott, A.J. Olson, Software News and Update AutoDock Vina: Improving the Speed and Accuracy of Docking with a New Scoring Function, Efficient Optimization, and Multithreading. Journal of Computational Chemistry. 31 (2010) 455-461. doi:10.1002/jcc.21334.
49. M. Zusso, V. Lunardi, D. Franceschini, Ciprofloxacin and levofloxacin attenuate microglia inflammatory response via TLR4/NF-kB pathway. J Neuroinflammation. 16 (2019) 1-12. doi:10.1186/s12974-019-1538-9.
50. A. Kashyap, P.K. Singh, S. Satpati, H. Verma, O. Silakari, Pharmacophore modeling and molecular dynamics approach to identify putative DNA Gyrase B inhibitors for resistant tuberculosis. J Cell Biochem. 120 (2019) 3149-3159. doi:10.1002/jcb.27579.
51. A. Ioanoviciu, S. Antony, Y. Pommier, B.L. Staker, L. Stewart, M. Cushman, Synthesis and mechanism of action studies of a series of norindenoisoquinoline topoisomerase I poisons reveal an inhibitor with a flipped orientation in the ternary DNA-enzyme-inhibitor complex as determined by X-ray crystallographic analysis. Journal of Medicinal Chemistry. 48 (2005) 4803-4814. doi:10.1021/jm050076b.
52. X. Chi, P. Yang, E. Zhang, Significantly increased anti-tumor activity of carcinoembryonic antigen-specific chimeric antigen receptor T cells in combination with recombinant human IL-12. Cancer Med. 8 (2019) 4753-4765. doi:10.1002/cam4.2361.
53. X. Sun, Q. Deng, Z. Liang, Cigarette smoke extract induces epithelial-mesenchymal transition of human bladder cancer T24 cells through activation of ERK1/2 pathway. Biomed Pharmacother. 86 (2017) 457-465. doi:10.1016/j.biopha.2016.12.022.

Journal Pre-proofs

Fig-1. Schematic diagram of overall design simulation of quinolone derivatives

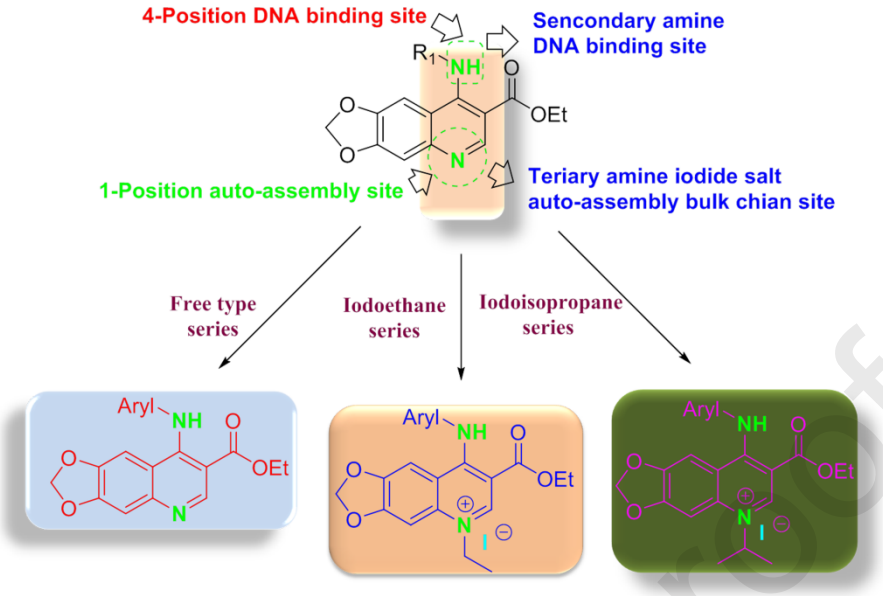

Journal Pre-proofs

Fig 2. 3D binding mode of derivative 12 in the binding site of (a) Human topoisomerase I (PDB ID: 1TL8); (b) *S. aureus* DNA gyrase (Topo II, PDB ID: 2XCT).

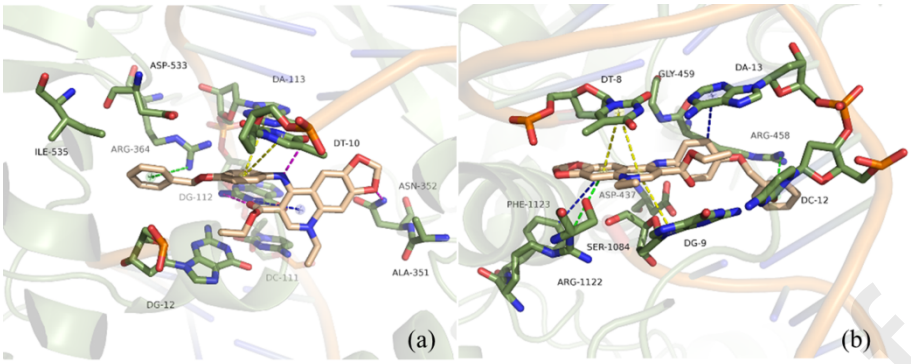

Journal Pre-proofs

Scheme-1. General synthetic route of quinolone derivatives

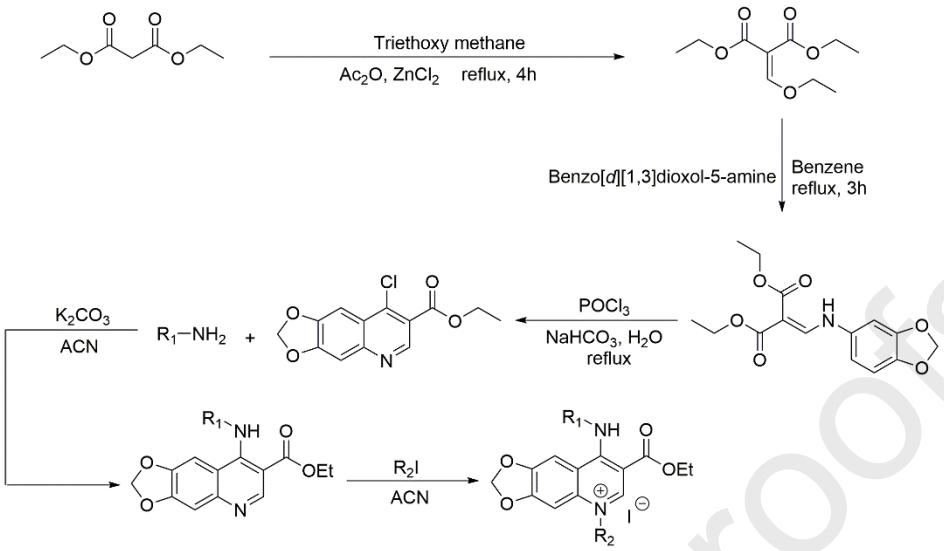

1 $\mathbf{R_1}$ = -CH_2Ph

2 $\mathbf{R_1}$ = -CH_2CH_2Ph

3 $\mathbf{R_1}$ = -$CH_2CH_2Ph(OCH_3)_2$

4 $\mathbf{R_1}$ = -$PhOCH_2Ph$

5 $\mathbf{R_1}$ = -CH_2Ph; $\mathbf{R_2}$ = -CH_2CH_3

6 $\mathbf{R_1}$ = -CH_2CH_2Ph; $\mathbf{R_2}$ = -CH_2CH_3

7 $\mathbf{R_1}$ = -$CH_2CH_2Ph(OCH_3)_2$; $\mathbf{R_2}$ = -CH_2CH_3

8 $\mathbf{R_1}$ = -$PhOCH_2Ph$; $\mathbf{R_2}$ = -CH_2CH_3

9 $\mathbf{R_1}$ = -CH_2Ph; $\mathbf{R_2}$ = -$CH(CH_3)_2$

10 $\mathbf{R_1}$ = -CH_2CH_2Ph; $\mathbf{R_2}$ = $CH(CH_3)_2$

11 $\mathbf{R_1}$ = -$CH_2CH_2Ph(OCH_3)_2$; $\mathbf{R_2}$ = -$CH(CH_3)_2$

12 $\mathbf{R_1}$ = -$PhOCH_2Ph$; $\mathbf{R_2}$ = -$CH(CH_3)_2$

Journal Pre-proofs

Table-1. In vitro growth inhibitory activity (IC_{50}μM) of compounds 1-12 against human lung cancer cell line (A549), human hela cell line (HeLa), human gastric carcinoma cell line (SGC-7901), normal liver L-02 cell line (L02) by MTT assay.

Compounds	IC_{50}			
	A549	Hela	SGC-7901	L-02
1	31.31±6.25	73.25±6.55	>120	>200
2	94.31±4.63	73.97±4.83	>120	>200
3	46.51±18.96	>120	>120	>200
4	17.75±0.95	>120	>120	>200
5	82.46±2.49	57.32±2.77	84.93±7.49	140.86±10.35
6	>120	>120	>120	>200
7	59.36±7.95	35.56±0.87	110.72±2.52	131.33±7.10
8	12.34±1.48	7.22±0.48	29.72±5.79	13.57±1.41
9	57.32±14.24	51.18±2.94	73.39±4.18	131.77±8.08
10	>120	>120	>120	>200
11	90.00±3.21	68.58±4.96	>120	>200
12	5.18±0.64	7.62±1.05	17.59±0.41	54.45±4.88
5-FU	98.55±0.72	109.65±2.81	113.04±1.07	>200
MTX	60.25±9.14	107.29±1.97	84.05±7.47	185.80±13.10

IC_{50}: Each value was averaged by three parallel groups of eight repeats and calculated using a SigmaPlot software.

Journal Pre-proofs

Table-2. Antibacterial screening in terms of the MIC (μg/mL**)** for the tested compounds in reference to Ampicillin and Ciprofloxacin, respectively.

Compound	MIC[a] / (nmol·mL^{-1})		ClogP[b]
	Escherichia coli	*Staphylococcus aureus*	
1	> 50	> 50	2.53
2	25	50	1.56
3	> 50	25	2.18
4	6.25	6.25	2.09
5	25	25	2.43
6	3.125	25	1.20
7	12.5	25	2.02
8	3.125	3.125	2.04
9	25	6.25	3.13
10	6.25	6.25	2.58
11	25	6.25	3.26
12	3.125	3.125	2.83
Amoxicillin	50	25	
Ciprofloxacin	25	12.5	

[a]MIC minimum inhibitory concentration;

[b]calculated on ACD/Labs website.

Journal Pre-proofs

Highlights.

- The target compounds, 5–12, exhibited significant antitumor and antibacterial activity.
- Compound 12 was found to be the most potent derivative with IC_{50} values.
- Compound 12 had the most potent inhibitory activity.

Graphical Abstract

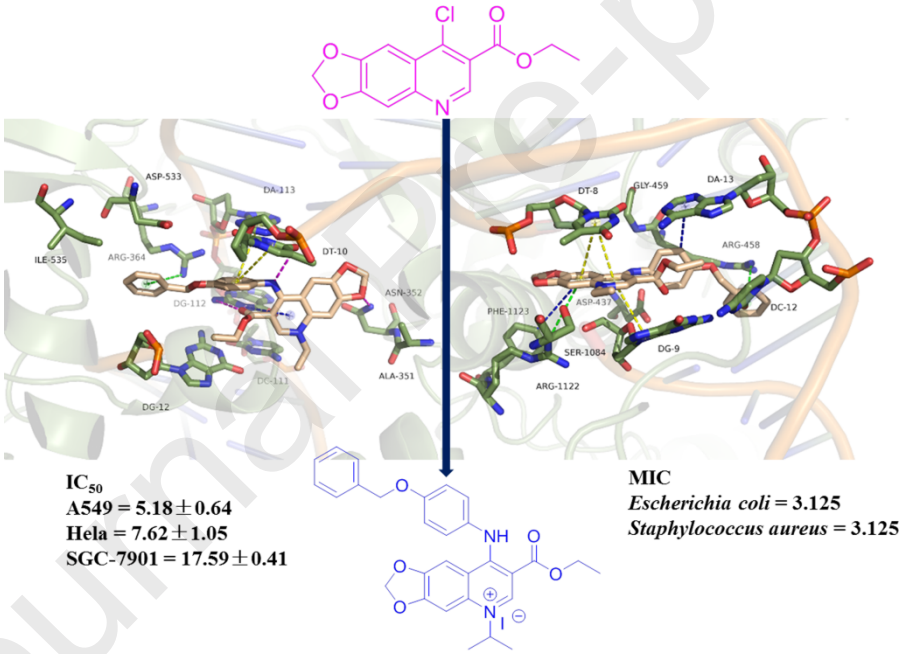

Journal Pre-proofs

Declaration of interests

☒ The authors declare that they have no known competing financial interests or personal relationships that could have appeared to influence the work reported in this paper.

☐The authors declare the following financial interests/personal relationships which may be considered as potential competing interests:

Journal Pre-proofs